

Computed Tomography

CT.1 Historical Background. Johann Radon showed in 1917 that 2-D section images could be reformulated using mathematical transformation of projection data (i.e. using a Radon transform). Projection data are line integrals (summations of image values) recorded across an object at some angle (Figure 1). The link between projection data and x-ray images (maps of the effects of attenuation) was not obvious. However, motivation was high since section x-ray images would have the ability to make high contrast section images of the body by removing interference from overlapping tissues. Later in this chapter we will see how the projection dilemma was resolved. Even with the knowledge of how to make x-ray images into projections, imaging instrumentation and computing power was not able to provide this capability early on, so we had to wait many years for technology to catch up with the theory. By the 1960s several research labs were able to reconstruct x-ray section images from x-ray projections acquired from physical objects, and these successes spurred intensive research into devices that could be used in humans. In the 1970s x-ray computed tomography (CT) was formally introduced for clinical use, which was followed by rapid technological refinement. Since reconstructed images looked like the thinly sliced tissue sections used for microscopic inspection, the term "Tomography", literally meaning a picture of a cut section, was adopted, and early x-ray tomographic imaging systems were called Computed Axial Tomographic or "CAT" scanners. However, common use has dropped this designation in favor of computed tomography or just CT. In 1979 two early researchers in the field, A. M. Cormack and Godfrey Hounsfield, were jointly awarded the Nobel Prize for Computed Tomography.

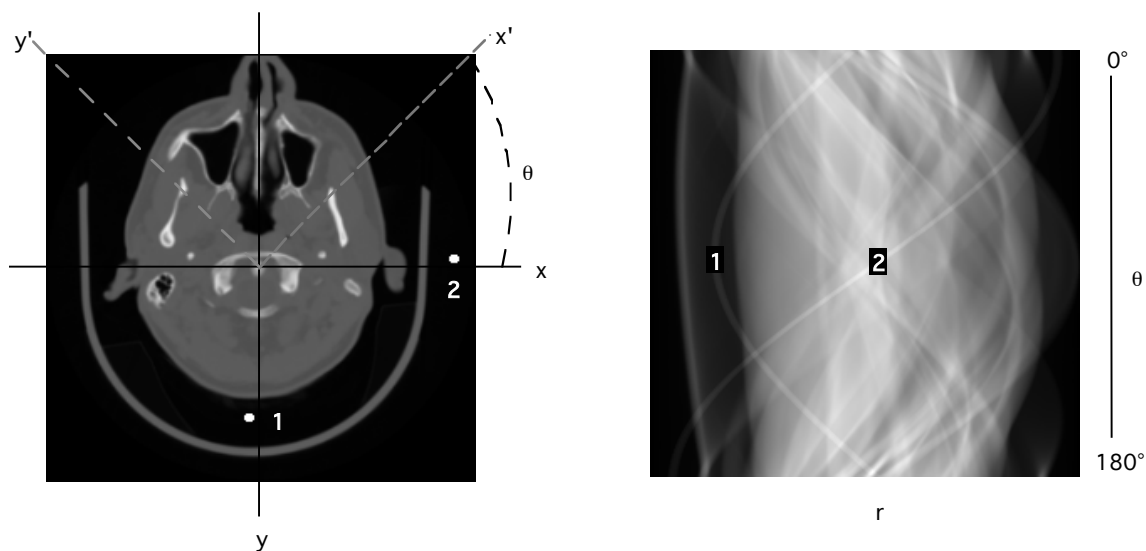


Figure 1. A CT image (a) and its projections $p_\theta(r)$ (b) presented as an image called a sinogram.

Figure 1b illustrates the set of projections $[p_\theta(r)]$ for $\theta = 0$ to 180 degrees from the CT image in 1a. The top row in 1b is at 0 degrees and the bottom row at 180 degrees. Columns (r) index positions within projections. Sinusoidal paths formed by landmarks 1 & 2 lead us to call this image a sinogram. The 0 -degree projection is a view from the bottom, while the 90 -degree

projection a view from the right. Values at each r in projection $p_\theta(r)$ are the result of integration across the object along a line perpendicular to the projection (i.e. line integrals).

The goal of CT imaging of the body is to obtain a set of 2-D serial section images, $o_n(x,y)$, from the body's 3-D object $o(x,y,z_n)$. During reconstruction the z extent of the object (Δz) is collapsed into a 2-D section image. For simplicity, a tomographic image will always be treated as a 2-D function realizing that integration along the z -extent of each section image is involved.

CT.2 Theory. Fourier transform theory provides a good theoretical approach to understanding the Radon transform and more generally tomographic reconstruction of images from projections. The basis for this explanation is provided in the following equations:

$$O(u, v) = \iint o(x, y) e^{-2\pi i(ux+vy)} dx dy \tag{CT-1}$$

$$O(u, v) = \mathfrak{F}\{o(x, y)\} \tag{shorthand notation}$$

$$o(x, y) = \iint O(u, v) e^{2\pi i(ux+vy)} du dv \tag{CT-2}$$

$$o(x, y) = \mathfrak{F}^{-1}\{O(u, v)\}$$

where the integration is performed over the domains of $o(x,y)$ and $O(u,v)$. These equations (seen in earlier chapters) form a Fourier transform pair. Either $O(u,v)$ or $o(x,y)$ can be calculated from the other and therefore each must contain a complete description of the object they represent (Figure 2). Conceptually if we are able to obtain $O(u,v)$ then we can then compute $o(x,y)$ using Eq. CT-2. The following discussion focuses on how to obtain $O(u,v)$ from projections.

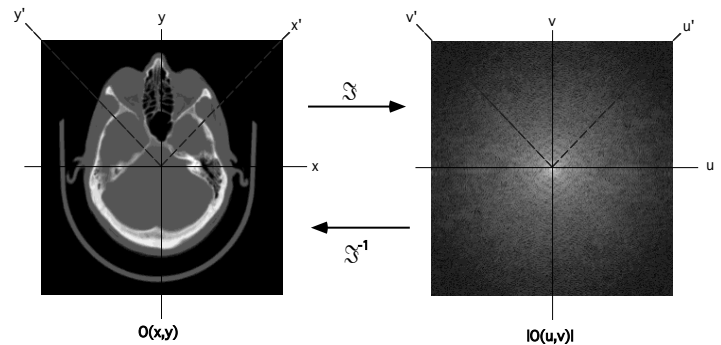


Figure 2. The spatial domain $o(x,y)$ and frequency domain $|O(u,v)|$ representations for a head CT study. $\text{Log}_{10} |O(u,v)|$ was used in this figure to better illustrate the higher frequency terms.

Figure 2 illustrates the correspondence between spatial and frequency domain representations of a CT section image in the head. Coordinate origins are assigned to the center of the image arrays for both domains. This is taken to be the axis of rotation for imaging (x-ray CT, SPECT, and PET). Image spatial coordinates (x,y) are expressed in mm and corresponding frequency coordinates (u,v) in lp/mm. While the spatial object function $o(x,y)$ is always real, the frequency object function $O(u,v)$ is usually complex. Only the magnitude of $O(u,v)$ is illustrated, but in general it is composed of both a magnitude and phase (or real and imaginary) parts.

The equation for mapping a point in the x - y image to a point in the r - θ sinogram (Figure 1) is as follows:

$$r(\theta) = r_{xy} \cdot \cos(\phi - \theta) \tag{CT-3}$$

where

$$r_{xy} = \sqrt{x^2 + y^2} \quad \phi = \tan^{-1}\left(\frac{y}{x}\right)$$

with r_{xy} the distance from the origin to the point x,y , ϕ the counter-clockwise (CCW) angle from the positive x -axis to the point, and θ the angle of the projection. The three parameters of Eq. CT-3 determine the key features of the sinusoidal path followed by a point in the object:

- The amplitude of the sinusoid is equal to its distance from the axis of rotation (r_{xy}).
- The phase of the sinusoid is determined from its starting phase ϕ .
- The sinusoid is theoretically fully defined over a range of θ from 0 to π or 180 degrees.

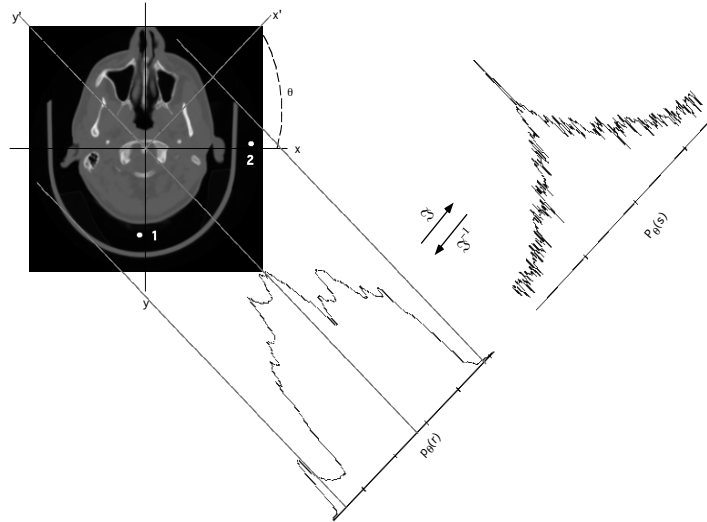


Figure 3. Formation of a projection $p_0(r)$ and the magnitude of its Fourier transform $P_0(s)$.

The feature of the Fourier transform that provides greatest insight into transforms needed for computed tomography is the **central slice theorem**. This theorem states that the Fourier transform of the projection $p_\theta(r)$ in the spatial domain is identical to the profile $P_\theta(s)$ in the 2-D Fourier domain (Figure 3). Here “ r ” corresponds to the distance from the origin measured in the spatial domain and “ s ” the distance from the origin in the spatial frequency domain. A calculation of the frequency domain profile from Eq. CT-1 where $v = 0$ is helpful to illustrate this relationship:

$$O(u, 0) = \iint o(x, y) e^{-2\pi i u x} dx dy \tag{CT-4}$$

where the order of integration can be interchanged yielding

$$O(u, 0) = \int \left[\int o(x, y) dy \right] \cdot e^{-2\pi i u x} dx . \tag{CT-5}$$

The term within the bracket is the summation or integration of $o(x,y)$ over all y holding x constant (a line integral for each x). This is called the projection of the object, calculated perpendicular to the x -axis. This projection can be referred to as $p_0(x)$ and this leads to:

$$P_0(u, 0) = O(u, 0) = \int p_0(x) e^{-2\pi i u x} dx \tag{CT-6}$$

Eq. CT-6 shows that the profile $P_0(u,0)$ in the frequency domain at $v = 0$ corresponds to the 1-D Fourier transform of the projection $p_0(x)$ in the spatial domain. Both the projection and the

profile correspond to data acquired at $\theta = 0$. A more general equation for the frequency domain profile is:

$$P_{\theta}(s) = \int p_{\theta}(r)e^{-2\pi i r s} dr \quad (\text{CT-6a})$$

The profile $P_{\theta}(s)$ is a central profile because its origin coincides with the origin in the frequency domain. Eq. CT-6a can be shown to be true at any angle. As stated previously if we can acquire data to determine the 2-D Fourier transform of the object $O(u,v)$ we can reconstruct it using Eqn. CT-2. The task is then to fill in the 2-D Fourier space by acquiring a complete set of projections about the object, and this can be done using projections spanning 0-180 degrees. The following points summarize the theoretical requirements and basis for tomographic reconstruction in computed tomography:

- Projections $p_{\theta}(r)$ are summations along a line, or line integrals of the object function values, at projection angles θ .
- For each spatial domain projection $p_{\theta}(r)$ there is a corresponding frequency domain central profile $P_{\theta}(s)$. Central Slice Theorem.
- If a sufficient number of spatial domain projections are acquired then a sufficient number of central profiles $P_{\theta}(s)$ can be calculated to properly complete the 2-D Fourier domain. An inverse Fourier transform can be used to calculate $o(x,y)$ from equation CT-2.

These points help to explain how a tomographic image can be calculated from projections. There are various methods to acquire data and x-ray and nuclear medicine computed tomographic images, but all are based on this basic mathematical description of computed tomography. Several will be discussed later in this chapter.

A challenge for CT image acquisition is to acquire projection data that effectively fill the 2-D frequency domain. It is necessary that the acquired data conform to the definition of a projection. A projection can be mathematically defined using a delta function as

$$p_{\theta}(r) = \iint o(x,y)\delta(r - x\cos(\theta) - y\sin(\theta))dxdy \quad (\text{CT-7})$$

To help understand the arguments of the delta function in this equation we need the correspondence between locations in unrotated (x, y) and rotated (x', y') coordinate systems. The mathematical relationship for a CCW rotation of angle θ about the origin is determined using the following transform matrix format:

$$\begin{bmatrix} x' \\ y' \end{bmatrix} = \begin{bmatrix} \cos(\theta) & \sin(\theta) \\ \sin(-\theta) & \cos(\theta) \end{bmatrix} \begin{bmatrix} x \\ y \end{bmatrix} \quad (\text{CT-8})$$

From CT-8 we see that $x' = x \cos(\theta) + y \sin(\theta)$. Integration in CT-7 is therefore constrained to be along a line $r = x'$ by $\delta(r-x')$ which is parallel to the y' axis (see Fig. 3). The rotational origin for x-ray CT is the axis of rotation or the axis about which projections are acquired. Equation CT-8 can be used for backprojection and reprojection algorithms since given x', y' , and theta we

can calculate x and y . During projection for each x' (or r) we sum along y' to calculate $p_{\theta}(r)$. For backprojection we divide the projection data $p_{\theta}(r)$ equally along y' .

In x-ray and nuclear medicine tomographic imaging a set of projections $p_{\theta}(r)$ are usually acquired by rotation of the imaging device through a series of angles (θ) about the object. Since the projection at angle θ should be identical to that at angle $\theta + 180^{\circ}$, only 180° scanning is required. This is confirmed by the fact that the 2-D Fourier space can be completely filled with profiles spanning 180 degrees. For various reasons, the scan angle extent is usually larger than 180° . However, angular extent smaller than 180° will not completely fill the 2-D Fourier space of the object and leads to reconstruction errors. **Note:** Incomplete filling of the 2-D Fourier space can be partly compensated by interpolating values between missing profiles or reducing the highest frequency used during reconstruction, but both lead to reduced spatial resolution.

As stated in the introduction a projection must be composed of line integrals (i.e. summation) of object values. This requirement is especially important in x-ray CT since raw projection data are the intensity of the x-rays transmitted through the object, not an integration of object values. To understand how x-ray CT projection data are converted to a proper set of line integrals summing object values, the characteristics of the raw x-ray projection data need to be analyzed. The x-ray intensity at a location r in a projection is modeled as follows:

$$I_{\theta}(r) = I_0(r) e^{-\iint \mu(x,y) \delta[r - x \cos(\theta) - y \sin(\theta)] dx dy} \quad (\text{CT-9})$$

where $I_0(r)$ is the intensity at “ r ” without the object and $\mu(x,y)$ the linear attenuation coefficient at object location x,y . Dividing both sides of Eq. CT-9 by $I_0(r)$ and taking the natural logarithm leads to an equation for the integral of linear attenuation coefficients, i.e. projection $p_{\theta}(r)$ along a line defined by $x' = r$:

$$p_{\theta}(r) = \ln\left(\frac{I_{\theta}(r)}{I_0(r)}\right) = -\iint \mu(x,y) \delta(r - x \cos(\theta) - y \sin(\theta)) dx dy \quad (\text{CT-10})$$

For x-ray CT the raw projection data is converted logarithmically to proper projection data using equation CT-10. Inspection of Eq. CT-10 shows that in x-ray CT the values computed during reconstruction are linear attenuation coefficients (μ).

While x-ray CT calculates images that are linear attenuation coefficients, a different scheme was devised to help standardize CT numbers. Hounsfield suggested that it would be useful to report CT values as relative attenuation with the attenuation coefficient of water being the reference point. This ultimately led to the following equation for CT numbers:

$$CT\# = \frac{\mu - \mu_{\text{water}}}{\mu_{\text{water}}} \times 1000$$

Inspection of $CT\#$'s shows that the $CT\#_{\text{water}} = 0$ and $CT\#_{\text{air}} = -1000$. Since the linear attenuation of fat is less than that of water $CT\#_{\text{fat}} < 0$. Most other soft tissues are positive, while that of dense bone can be as high as 3000. The adoption of CT numbers has helped to simplify communication of image values in x-ray CT. Importantly, when properly calibrated CT numbers

can be less sensitive to changes in kVP and beam filtration than are linear attenuation coefficients. Can you explain why?

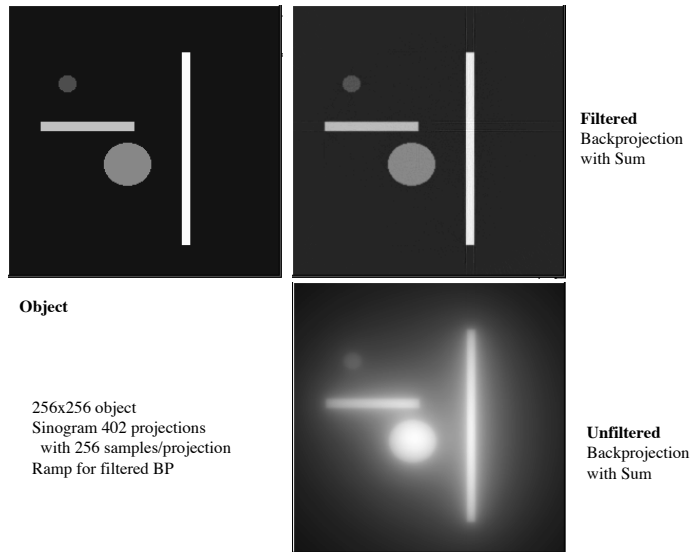


Figure 4. Filtered backprojection image is a faithful reproduction while simple (unfiltered) backprojection image is blurred.

While there are several approaches to determine $o(x,y)$ from $O(u,v)$, the most basic, though not mathematically correct, is called simple backprojection. Simple backprojection is an attempt to redistribute line integral data into the object. Backprojection uniformly redistributes the line integral values within a circle of diameter equal to the length of the projections. This circle is called the scan circle. The entire object must reside in the scan circle to be correctly reconstructed, otherwise it will not be sampled at each projection. Simple backprojection (unfiltered backprojection) fails to correctly reconstruct the object from its projections (Figure 4).

This is easy to understand from the following example:

Example 1. If a point-like object (centered in the scan circle) is imaged, each projection will be identical, having data only at its center. Backprojection of the first projection divides its value (sum of image data) equally along a line through the origin within the scan circle. A similar uniformly filled line will be backprojected for each projection angle. During each backprojection new values are added to previous values. At the center of the image each backprojection contributes to the sum; however, backprojections still sum further away from the center. Therefore, the image of the point source reconstructed using such simple backprojection is blurred. This image is in fact the point spread function (psf) of image formation using simple backprojection (Figure 5). This psf diminishes with distance from the center following a “ $1/r$ ” trend, and results from the overlapping of backprojected lines, where all lines overlap at the origin.

There is another way to look at the problem associated with simple backprojection. If simple backprojection worked properly then reprojection from the backprojected image should produce projections identical to those from the real object. This cannot happen due to the overlapping of different projections, which produce non-zero values of line integrals away from the center or origin during reprojection. The only solution to this dilemma is for the projection data to be modified to include both positive and negative values to remove such. This will become obvious soon.

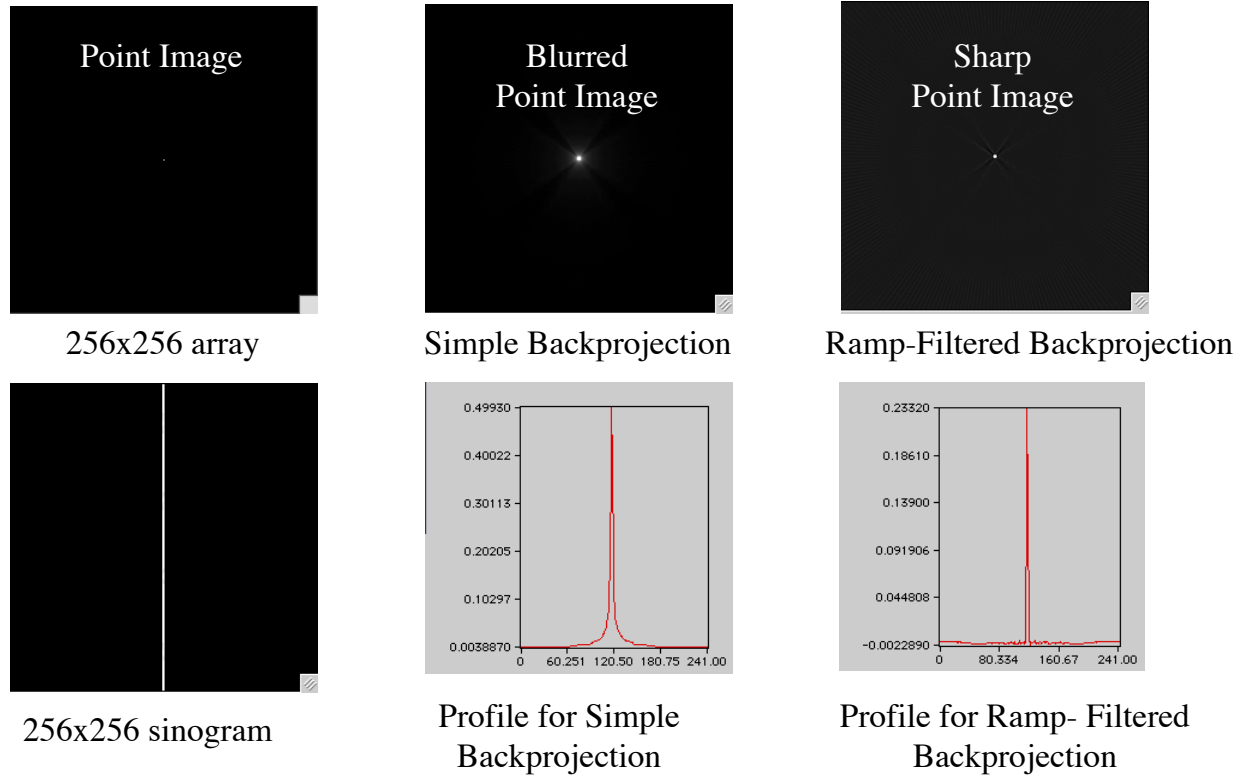


Figure 5. Comparison of point spread functions for simple and ramp-filtered backprojection methods.

While simple backprojection forms a blurred version of the object (middle Fig. 5), a special ramp-filtered backprojection approach (right Fig. 5) produces a nearly perfect replica of the object. The origin of this problem can be seen by inspection of the point spread function of simple back projection (Figure 5). The profile through this spread function reveals that the simple backprojection $psf(r)$ drops off as $1/r$. There are two approaches to remove the blurring introduced by this $1/r$ broadening of $psf(r)$. One method to correct for the blurring is to deconvolve the simple backprojection image with an appropriate function in the spatial domain. However, this is not the most straightforward approach, and a Fourier domain approach is usually preferred. Blurring in the spatial domain is described mathematically as follows:

$$i(x,y) = o(x,y) \otimes \otimes psf(x,y) \tag{CT-11}$$

where $psf(x,y) = k/r$ and $r = (x^2 + y^2)^{1/2}$. The corresponding equation in the Fourier domain is

$$I(u,v) = O(u,v) STF(u,v). \tag{CT-12}$$

where $STF(u,v) = K/\rho$, $\rho = (u^2 + v^2)^{1/2}$. This STF shows a net reduction in frequency response as $\sim 1/\rho$ for simple backprojection. For realistic point spread functions, neither k/r nor K/ρ go to ∞ as their denominators go to zero. In fact for real CT the value of K/ρ is equal to an integral about k/r near $r=0$. We will see how this can be calculated for discrete CT data later. The drop off in frequency response in $I(u,v)$ can be correctly compensated by multiplication of $I(u,v)$ by the inverse of STF which is ρ/K to calculate $O(u,v)$ as follows:

$$O(u,v) = I(u,v) \cdot \rho/K \quad (\text{CT-13})$$

The ρ/K term is a straight line when plotted as a function of ρ and is therefore referred to as a “ramp” filter, and the processing indicated in Equation CT-13 is called “ramp filtering”. The ramp filter compensates for the drop in high frequency response due to the oversampling of low frequencies, or undersampling of high frequencies associated with summation and backprojection.

Ramp filtering is generally done on a projection-by-projection basis to provide filtered projections as follows

$$p'_\theta(r) = \mathcal{F}^{-1}[P_\theta(s) |s|/K] \quad (\text{CT-14})$$

where $|s|$ is equivalent to ρ from equation CT-13. Backprojection of $p'_\theta(r)$ is called ramp filtered backprojection and its effect is to create an almost perfect reconstruction (Figure 5).

A more intuitive description of the requirement of a ramp filter for proper CT reconstruction from projections follows from inspection of $p_\theta(r)$, $P_\theta(s)$ and $\text{PSF}(u,v)$ for a point object $\delta(x,y)$. For a perfect CT imager, i.e. no unsharpness, each $p_\theta(r)$ will be a 1-D delta function $\delta(r)$ and its Fourier transform, $P_\theta(s)$, will be a constant = 1. To model simple backprojection with summation in the u,v domain each $P_\theta(s)$ must be summed into the u,v domain at the proper angle. This means that the response at the origin [$\text{PSF}(u=0,v=0)$] will be equal to N_p where N_p is the number of projections overlapping at the origin, since the central slice theorem states that all $P_\theta(s)$ go through the origin. Also, $\text{PSF}(u,v)$ will fall off as $1/|s|$ moving away from the origin. This is because at each radial distance from the origin $2N_p$ projections are summed along a circle of circumference = $2\pi\rho$, so the magnitude drops off with increasing radius as $N_p / \pi|s|$ ($|s|$ and ρ are used synonymously). To achieve a constant frequency response (the correct Fourier transform of $\delta(x,y)$) then $\text{PSF}(s)$ must be multiplied by a frequency compensation term like $\pi|s|/N_p$. While this description does not exactly match that in Eq. CT-13, the difference falls out with normalization of the final data.

Note: If the $P_\theta(s)$ were put into the u,v domain as an average rather than a sum the compensation would occur automatically.

The 2-D Fourier transform of $\delta(x,y)$ should be uniform across the u,v frequency space. The need to increase magnitude as a function of frequency stems from the fact that while each profile can have uniform frequency response, when summed into the 2-D Fourier space the net magnitude falls off following $1/\rho$. Compensation for this high frequency drop off results in ‘equalized’ frequency response and explains the necessity for the ramp filter. Since it is simpler to perform the filtering in 1-D, Equation CT-14 is usually used. Also, when using this technique, reconstruction can be done during data acquisition, where each acquired projection is filtered and backprojected as soon as it is acquired. Reconstructed slice images are available almost immediately following the acquisition of a complete set of projection data. Filtered backprojection implements the Radon transform.

It is certainly possible to reconstruct $o(x,y)$ directly from $O(u,v)$ by taking the inverse Fourier transform bypassing the need for filtered backprojection. However, unlike filtered backprojection where backprojection can be done immediately following acquisition of each new projection, the inverse Fourier transform method must wait until all projections have been transformed to Fourier space, i.e. the end of the scan. Early systems were very slow and filtered backprojection soon became the preferred approach. It should be noted that filling in $O(u,v)$ from Fourier transform of projections can be done carefully to avoid summing at the origin. One way to do this is to sum and fill normally, but save a buffer of how many entries were made, and correct to the average values once all projections are acquired.

Projection data do not have to be acquired using parallel lines for integration. For improved geometrical efficiency fan beam geometry is commonly used in x-ray CT. The fan beam line integrals can be sorted into parallel projections before processing or processed using a different filter. However, all discussions in this chapter focus on parallel beam type projections and reconstructions.

CT.3 Practical Considerations.

CT.3.1 Number of Samples per Projection. The number of samples per projection, N_s , can be estimated using Shannon’s sampling theorem. Recall that this theorem specifies that the sampling frequency $f_s \geq 2 f_{max}$ where f_{max} is the highest frequency or bandwidth limit of the imaging system. The number of samples per projection based on the sampling theorem is

$$N_s = 2f_{max} \times FOV \tag{CT-15}$$

Example 1: For some CT $f_{max} \sim 1$ lp/mm and $FOV = 256$ mm, so $N_s = 512$ samples.

Example 2: For Nuclear Medicine using single photon emission computed tomography (SPECT) images with $f_{max} \sim 1$ lp/cm $N_s = 50$ for 25 cm FOV (would likely use 64) and $N_s = 80$ for a 40 cm FOV (would likely use 128).

CT.3.2 Number of Projections.

The number of projections (N_p) is calculated to ensure complete filling of the u,v space up to the highest frequency. This is accomplished if the number of samples/distance along the largest circle in u,v space is equal to number of samples/distance along the radial direction. The number of samples in a projection N_s determines the u & v dimension of the corresponding Fourier space (# rows, # columns).

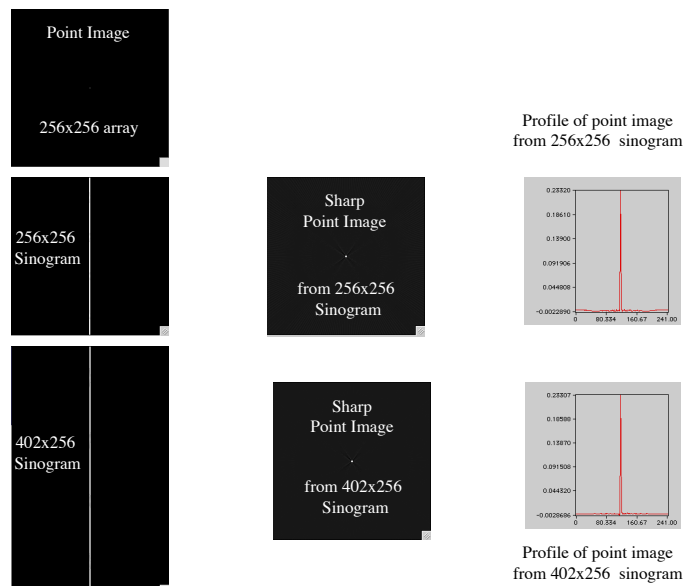


Figure 6. Example shows improvement in background around reconstructed point when number of projections $N_p = \pi/2 \cdot N_s$ where N_s is the number of samples per projection.

N_s therefore determines the number of points in the diameter of the largest circle in u,v . The number of points needed along the circumference of this circle to keep samples/distance constant is $\pi \times$ diameter or πN_s . Since each projection profile provides two points along this circumference the minimum number of projections is one-half this value or

$$N_p = \pi/2 \cdot N_s \tag{CT-16}$$

Figure 6 illustrates the improvement in a reconstructed point following the guideline given in Eq. CT-16. The total number of line integrals acquired is the number of samples per projection times the number of projections = $N_s N_p$. The following table summarizes some common combinations of N_s and N_p :

Application	N_s	N_p	# line integrals
Nuc Med	64	101	6464
Nuc Med	128	201	25,728
x-ray CT	512	804	411,648
x-ray CT	1024	1608	1,646,592

These table values may be larger or smaller depending on the many factors, including different detector design and spatial resolution needs.

CT.3.3 Net CT Filter Response. Though the mathematical form of the ‘ramp’ filter for theoretically correct CT reconstruction is well known, in most cases the net filter must be modified to reduce output at higher frequencies where SNR is often very low. This is accomplished using a low-pass filter. The bandwidth of the low pass filter is user selectable, though most x-ray CT consoles only provide options such as high, medium, and low-resolution filters. PET and SPECT systems generally provide a wider range of filters. A common low-pass filter is a Butterworth filter. It is a two-parameter filter and has a frequency response as follows

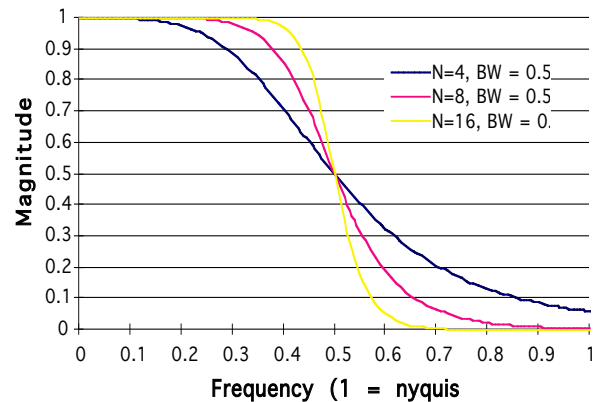


Figure 7. Butterworth filter frequency response.

$$Butterworth(u) = \frac{1}{1 + \left(\frac{u}{u_0}\right)^{2N}} \tag{CT-17}$$

where u_0 is the frequency where the filter output = 1/2 (called the bandwidth of the filter) and N is the order of the filter. The filter shape around u_0 changes with increasing order (Figure 7). For large N the filter magnitude approaches 1 for values of $u < u_0$ and 0 for $u > u_0$. The selection of N is based on the frequency response needs away from the designated bandwidth. The bandwidth determines the point where 1/2 magnitude is desired.

The net frequency response is determined as the product of the ramp filter and the user-selected low-pass filter (Figure 8). The net filter response peaks somewhere below u_0 , tracks the ramp at lower frequencies, and tends to zero at higher frequencies.

Figure 9 shows the MTF and noise of a tomographic imager prior to application of the net ramp filter. It demonstrates the need to taper the output of the filter at high frequencies where the SNR is poor while following the theoretical ramp at lower frequencies.

Low-pass filtering is critical in nuclear medicine (SPECT & PET) because the projection data are often very noisy. In these cases the low-pass filter bandwidth is set at approximately 1/2 the Nyquist limiting frequency as illustrated in Figure 9. While such low-pass filters improve the SNR in reconstructed images they degrade resolution, with frequency response above u_0 being attenuated.

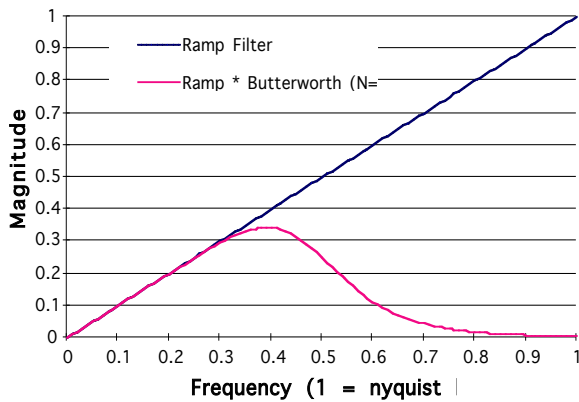


Figure 8. Ramp and net ramp modified by Butterworth filter.

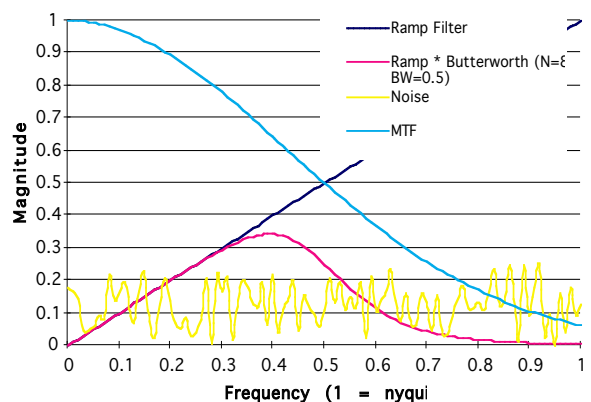


Figure 9. Noise and MTF determine the bandwidth to use for filtered ramp.

In x-ray CT similar low-pass filtering is done, but u_0 appears to be well above 1/2 of the Nyquist limit, since image detail is maintained with good SNR over a broader range of frequencies for most cases. Smoother images result for u_0 near 1/2 Nyquist limit with sharpness improving as u_0 is increased. The higher SNR at any given frequency for x-ray CT vs. Nuclear medicine CT systems is due to the much larger number of x-ray quanta acquired in x-ray CT.

CT.3.4 Beam Hardening. A problem that results from using a polyenergetic x-ray beam for CT is that the beam will be harder (mean energy higher) for thicker body regions, due to the longer attenuation path. The most common example of this is seen for imaging a cylindrical phantom (Figure 10). Note that higher mean energy means less attenuation and this is seen in a smaller linear attenuation coefficient μ .

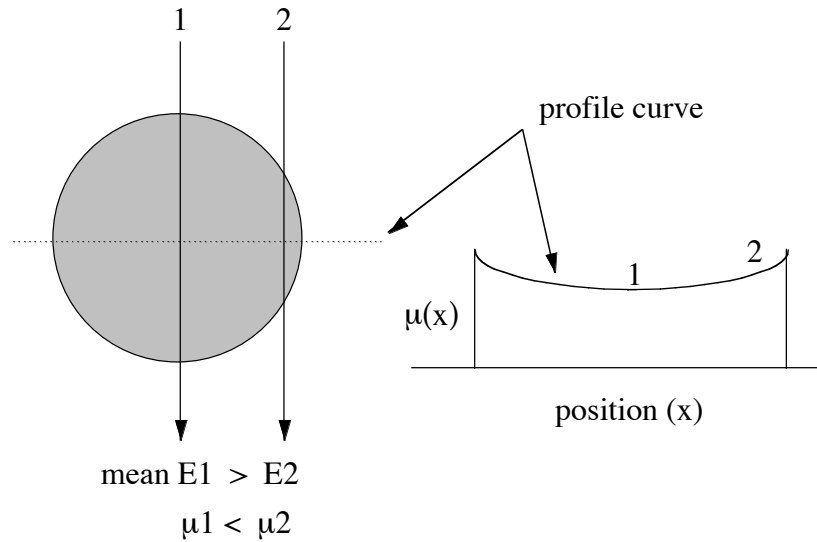


Figure 10. X-ray CT Beam hardening.

The profile of a reconstructed CT image will be darker in the middle since μ is proportional to CT#. The cupping seen in the graph of Figure 10 is the result of beam hardening in x-ray CT images.

There are several ways to resolve this beam-hardening problem. A commonly used method is to pre-harden the x-ray beam with extra aluminum filtration so that the additional hardening caused by the patient leads to a smaller percentage change in the mean x-ray beam energy. This

approach is supplemented by use of a higher KVP beam (125-130 KVP) than for routine projection radiographic imaging. A second method to reduce the beam hardening effect seen in Figure 10 is to use a “bow-tie” shaped aluminum filter to pre-harden the periphery (i.e. ray #2) more than the center of the beam (ray #1). This can be effective for cylindrical objects, but is not an acceptable general solution. A third method, and one not used much anymore, is to surround the object with a water bag. This was mostly used to reduce the dynamic range of x-ray intensity between detectors in the middle of the FOV and those at the periphery. Early CT detectors were limited in dynamic range, the ratio of highest to lowest x-ray intensity seen by the detectors.

A common method to correct for periphery-to-center beam hardening is based on a measured ratio of I_0 (no-attenuation signal) to I (attenuated signal). The logarithm of the ratio of I_0 to I if mean energy does not change should be a line of constant slope = μ when plotted versus diameter of a cylindrical water phantom (Figure 11). This follows from the simple equation describing attenuation of x-rays

$$\ln(I_0/I) = \mu d \tag{CT-18}$$

The graphical data from Figure 11 are used to correct measured values of $\ln(I_0/I)$ to theoretical values using a look-up table. In the example a value of $\ln(I_0/I) = 5$ would be mapped to a value of 6. This is a reasonably good method to correct the periphery-to-center beam-hardening problem for soft tissues and near cylindrical body sections. Some form of this correction is used on all x-ray CT machines.

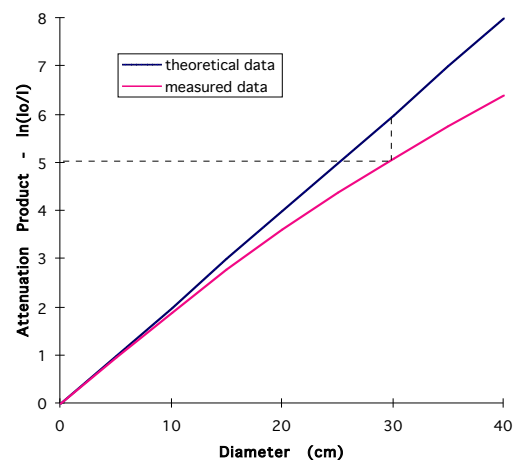


Figure 11. Beam hardening correction.

Another beam hardening problem often seen in head CT images comes from large differences in attenuation for rays traversing bone vs. soft tissue. This beam hardening cannot be well

corrected without some form of iterative processing. The result is a streak artifact near sharp edges of bone.

CT.4 Other Considerations.

Attenuation correction for SPECT and PET are required to provide true line integrals for projections. PET attenuation correction is quite good though SPECT attenuation correction is sometimes poor. Both can use 360-degree data acquisition, and this is needed for good attenuation correction. PET acquires multiple slices simultaneously. SPECT acquires multiple slices in one rotation. X-ray CT now can acquire multiple sections with high-speed helical scanners.

Helical CT uses interpolation from helical to parallel projections before reconstruction.

Fastest CT is a scanning electron beam with a stationary, large-diameter anode.

Homework.

1. Calculate the projections ($P_i(r)$ from Eq. CT-10) at 0° and 45° for a square object 10 cm on each side, if $\mu = 0.2 \text{ cm}^{-1}$. Use the coordinate system given in Figure 2.

2. You are working on a research project to build a micro CT system with x, y, and z spatial resolution of 10 microns and a field of view of 5 cm. The system uses a pencil beam that is scanned across the object and then the object is rotated. The object is translated (stepped) in the z direction and the process is repeated. What values would you select for each of the following and show how you arrived at your conclusion:

- Dimensions of x-ray beam
- Distance between steps in the z direction
- Number of samples per projection
- Number of projections
- Image matrix size
- Form of the reconstruction filter

3. A simple formula can be used to estimate the form of the ramp filter for filtering the Fourier transform of projections. Given that $\text{Ramp}(u) = 1/N_p$ @ $u = 0$ and $\text{Ramp}(u) = 1$ @ $u = u_{\max}$, show that

$$\text{Ramp}(u) = \left[\frac{1 - \frac{1}{N_p}}{\frac{N_s}{2}} \right] |u| + \frac{1}{N_p}$$

4. The mean linear attenuation coefficient for a 40 cm water phantom is 0.2 cm^{-1} . What is the dynamic range of x-ray intensity seen by the CT detectors? Can this range be properly recorded with a 16 bit binary data format?

5. You have been asked to determine the center of rotation (COR) of a SPECT camera. Explain how you might do this using Equation CT-3. Also, suppose that the SPECT camera is wobbling about its COR during rotation (maybe because of gravity), how might you detect this problem?